Micellization of Poly(ethylene oxide)–Poly(propylene oxide) Block Copolymers in Aqueous Solution

Per Linse

Physical Chemistry 1, Chemical Center, University of Lund, P.O. Box 124, S-221 00 Lund, Sweden

Received January 26, 1993; Revised Manuscript Received May 19, 1993

ABSTRACT: The micellization in an aqueous solution of polymers containing ethylene oxide (EO) and propylene oxide (PO) was modeled on the basis of a mean-field lattice theory for multicomponent mixtures of copolymers with internal states occurring in heterogeneous systems. The critical micelle concentration, the aggregation number, and the hydrodynamic radius, as well as their temperature dependence of these, were examined for a number of Pluronic triblock copolymers and for two related block copolymers. A semiquantitative description of the strong temperature dependence of these quantities as observed experimentally for Pluronic F127 [$(EO)_{99}(PO)_{65}(EO)_{99}$] was obtained. An increase in the molecular mass or a decrease in the EO/PO ratio was found to reduce the temperature at the onset of micellization at a given polymer concentration and accordingly to decrease the critical micellization concentration at a given temperature. A smaller critical micellar concentration was associated with a larger aggregation number. A similar trend was found when the molecular structure was changed from that of a triblock to a diblock copolymer. Segment density profiles indicate the Pluronic micelles to consist of a hydrophobic core composed mainly of PO and an outer layer composed of a mixture of EO and water, the EO density gradually diminishing with radial distance.

I. Introduction

Triblock copolymers of the PEO–PPO–PEO type [PEO and PPO are poly(ethylene oxide) and poly(propylene oxide), respectively], which are often referred to by their trademarks Pluronic, Proxanol, and Synperonic, constitute a class of polymers to which increasing attention has been directed during recent years.[1–17] Applications involving block copolymers of this type are partly based on the self-association phenomenon which this class of molecules exhibits in solution. The uses of Pluronic polymers range from drug delivery and steric stabilization in a number of different areas to the concentration and enhancement of hydrophobic trace contamination in polluted water sources.

In aqueous solution, block copolymers of this type have been shown to form micelles, provided that the ratio of the more hydrophobic PPO block to the more hydrophilic PEO block is suitable and that the temperature and concentration are sufficiently high. Furthermore, like other EO-containing nonionic polymers and low-molecular-weight surfactants, these copolymers display at elevated temperature a reduced solubility in aqueous solution, as manifested by the existence of a lower consolute point.

One of the most interesting properties of aqueous Pluronic solutions is that the micellization is strongly temperature dependent. This has been studied extensively with a variety of methods during the last few years.[2–15,17] Various properties of interest here are the critical micelle concentration (cmc), the fraction of polymer molecules in micellar form, the micellar aggregation number, and the size of the micelles, as well as the temperature dependence of these various properties. The cmc is a property of particular interest. Although the values for it reported in the literature vary substantially, the cmc clearly decreases with an increase in temperature.[7,8,11,12,17] The average aggregation number and the micellar size likewise increase with temperature, although the absolute values of these vary between different systems and even between different batches.

Certain theoretical aspects of micelle formation of dissolved block copolymers have been investigated recently.[18–22] A theoretical approach common to the studies here has been the *a priori* spatial separation of the two different blocks of the copolymer within the micelle. The lyophobic block of the copolymer is assumed to be located in the core and the lyophilic block to be located exclusively in an outer layer (corona) of the micelle. With one exception,[19] no solvent penetration into the micellar core was allowed in such studies and, again with one exception,[20] the segment density profiles were held constant within the different regions. By minimizing an expression for the free energy, determinations could be made of the cmc, micellar size, etc. Contributions to the free energy typically included the interfacial free energy, the free energy associated with the deformation of the blocks of the copolymer, various enthalpic and entropic mixing contributions, and in some cases the entropic cost of confining the block junctions to an interfacial region. An important aim of these investigations was to find scaling relations for aggregation number and micellar size.

In a recent study, we investigated theoretically, using a different theoretical approach,[17] the micellization of block copolymers of the Pluronic type. We employed a lattice theory for heterogeneous systems, one initially developed by Scheutjens and Fleer[23] and later adapted for the description of micelle formation[24,25] and of polymers displaying inverse temperature behavior.[26,27] The results obtained were in qualitative agreement with experimental data, the study also reproducing temperature-dependent micellization correctly. Moreover, the segment densities could be predicted as a function of the distance from the center of the micelle without the *a priori* assumption of the segments being located in different regions.

In this paper, an extended investigation of the micellization and the micellar structure is presented. The theoretical approach is the same as used in the previous study, although a slightly different set of interaction parameters for the EO–PO interaction is employed. The new set is more satisfactorily determined and has been derived by fitting calculated phase diagrams of the ternary PEO–PPO–water system to experimental ones. Furthermore, a number of Pluronic polymers of differing composition have been considered. It was found that both

0024-9297/93/2226-4437$04.00/0

the composition and the polymer architecture markedly affect micellization and the micelles that are formed.

A polymer model containing internal degrees of freedom[26] is employed in the study. This polymer model has been shown to be fruitful for modeling inverse temperature dependence in both homogeneous[26-29] and heterogeneous systems.[30-32] The polymer model takes account of the fact that different conformations of ethylene oxide groups differ in their dipole moments and that the more polar conformations are less numerous. The conformations are divided into two classes or states, one being more polar with a lower energy and a lower statistical weight and one being less polar (referred to as nonpolar), having a higher energy and higher statistical weight. This categorization is also consistent, e.g., with ^{13}C chemical shift measurements.[33] At low temperatures, the former class dominates and the effective polymer–solvent interaction is favorable, whereas at higher temperatures the latter class dominates, rendering the polymer–solvent interaction less favorable. Furthermore, the effective polymer–solvent interaction becomes more unfavorable as the polymer concentration increases.

The paper is organized as follows. In section II, the theory basic to the heterogeneous lattice model for polymers with internal degrees of freedom is outlined briefly. An account is also provided of the thermodynamic model applied to the micellization. In section III, the polymer model and the interaction parameters used in the investigation are dealt with. In section IV, the calculated results are presented. In the first part of the section the results for Pluronic F127 are considered. The F127 triblock copolymer is one of the larger polymers of the Pluronic family and is moreover the one for which of the most experimental data concerning micellization is available. The new set of EO–PO interaction parameters was found to improve the results for the model, although the picture was not unequivocal. The last two parts of section IV deal with the effects of varying the polymer composition and the architecture of the block copolymer, respectively. Finally, the paper ends in section V with a summary of the main conclusions.

II. Theory

A lattice theory for multicomponent mixtures of copolymers with internal degrees of freedom occurring in heterogeneous systems was presented previously.[27] Here we provide a shorter account of it, one adapted to spherical micelles.

Lattice. Consider a spherical lattice of infinite extension as illustrated in Figure 1. The concentrical layers, starting from the center, are numbered $i = 1, 2, ..., M$, each layer containing L_i lattice sites; the number of sites increases with i and is not necessarily an integer. Since within each layer the Bragg–Williams approximation of random mixing is applied, all the lattice sites in a layer are equivalent. The number of nearest-neighbor sites, z, the fraction of these sites in the same layer, λ_{ii}, and the fraction of these in adjacent layers $i' = i \pm 1$, $\lambda_{ii'}$, are dependent on the lattice topology. In the case of a planar hexagonal lattice, $z = 12$ and $\lambda_{ii} = 0.5$. We consider the case in which each site is occupied by one solvent molecule or by one polymer segment. Since there are no nearest neighbors in nonadjacent layers, i.e., $\lambda_{ii'} = 0$ if $|i - i'| > 1$, and since the flux constraint implies $L_i\lambda_{ii'} = L_{i'}\lambda_{i'i}$, $i' = i \pm 1$, the λ matrix describing the lattice topology is fully determined.

The lattice is completely filled by a mixture of two components (polymer and solvent). There are n_x molecules of component x, each molecule consisting of r_x segments.

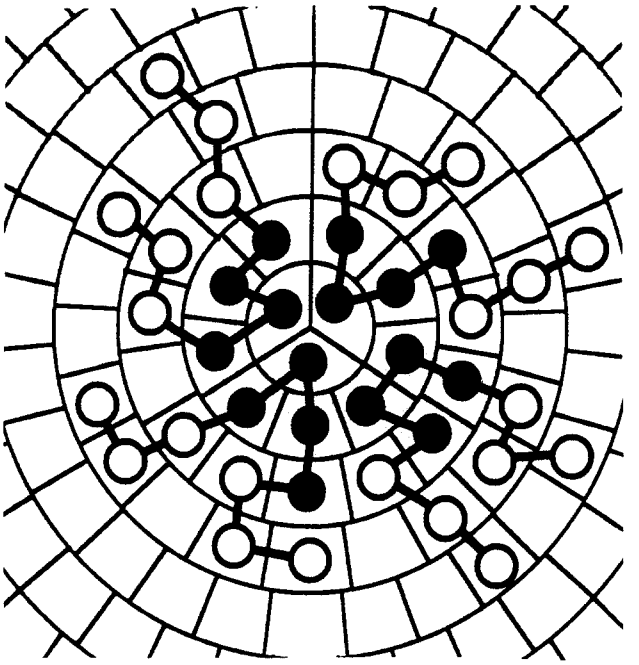

Figure 1. Two-dimensional illustration of an infinite spherical lattice and a micelle formed by four triblock copolymers, $B_3A_4B_3$. The hydrophobic segments A (filled circles) form the central part of the micelle, whereas the more hydrophilic segments B (open circles) form the outer layer of the micelle. Note the small number of unfavorable contacts between the hydrophobic segments and the solvent (unfilled lattice cells).

Since we are dealing with Pluronic block copolymers, two types of polymer segments are involved. The segment types, which will be referred to as species, are generically labeled A, A′, etc.

Conformation. Since the geometry of the lattice introduces a unique direction, the normal to the layer, the complete directional degeneration of spatial segment distributions in a homogeneous system is lifted. The various conformations of the polymer chains are distinguished in terms of the different ordering of their segments with respect to the layer numbers. Formally, a conformation c of component x is defined by an ordered set of layer numbers $k(x,s,c)$; $s = 1, r_x$ where $k(x,s,c)$ is the number of the layer in which the segment of rank s (the sth segment in the chain) of the component x in the conformation c is located (cf. Figure 1 which shows four chains, each being in a different conformation). With this definition, the degeneration of a component x in conformation c, neglecting self-exclusion, becomes $\omega_{xc}z^{r(x)-1}$ where

$$\omega_{xc} = L_{k(x,c,1)} \prod_{s=2}^{r_x} \lambda_{k(x,c,s-1),k(x,c,s)} \qquad (1)$$

$L_{k(x,c,1)}$ indicating the number of possibilities for the position of the first segment, being consistent with conformation c, and the product of λ elements representing the probability of the remaining $s - 1$ segments, likewise being consistent with conformation c.

Free Energy. The derivation of the internal state and of the segment distributions starts with the partition function of the model system. After replacement of the partition function with its largest term, the system's (Helmholtz) free energy relative to a reference state involving its separate amorphous components may be expressed as

$$\beta(A\text{-}A^*) = \beta(A_{int}\text{-}A^*_{int}) - \ln \frac{\Omega}{\Omega^*} + \beta(U\text{-}U^*) \qquad (2)$$

where $\beta = (kT)^{-1}$, k being Boltzmann's constant and T the

absolute temperature. The first term denotes the contribution arising from the internal degrees of freedom, the second term is the mixing entropy, and the third is the mixing energy.

Each state of a species is characterized by an energy term, U_{AB}, and a degeneration factor, g_{AB}, where in both cases A denotes the species and B the state of species A. The total internal free energy arising from the internal states becomes

$$\beta A_{int} = \sum_i \sum_A n_{Ai} \sum_B P_{ABi} \left[\beta U_{AB} + \ln \frac{P_{ABi}}{g_{AB}} \right] \quad (3)$$

where $\sum_i$ denotes the sum over layers, $\sum_A$ the sum over species (segment types), and $\sum_B$ the sum over the states of species A, n_{Ai} is the number of sites in layer i occupied by segments of type A, and P_{ABi} is the fraction of species A in layer i which is in state B. There are three contributions to the internal free energy, namely, U_{AB}, which is the internal energy of state B of species A; $-kT \ln g_{AB}$, where g_{AB} is the degeneration factor of state B of species A; and $kT \ln P_{ABi}$, an entropy term arising from the mixing of the states. In the case of EO (or PO), U_{AB} and g_{AB} describe the equilibrium between the polar and nonpolar states of EO (PO). Since the nonpolar state has a higher internal energy and greater degeneration, $U_{EO,nonpolar} > U_{EO,polar}$ and $g_{EO,nonpolar} > g_{EO,polar}$. Finally, A^* becomes zero by a suitable choice of reference state.

The mixing entropy arises from the difference between the configurational degeneration of the system and of the reference state. When self-exclusion at a mean-field level is taken into account and the contributions of all the conformations of all the components are included, the mixing entropy of the system can be expressed as

$$\ln \frac{\Omega}{\Omega^*} = -\sum_x \sum_c n_{xc} \ln \frac{n_{xc} r_x}{\omega_{xc}} \quad (4)$$

where n_{xc} denotes the number of chains of component x in conformation c and where ω_{xc}, which is related to the degeneration of component x in conformation c, is given by eq 1. In the case of a homogeneous system and of $r_x = 1$ for all x, in which $\omega_{xc} \to L$ and c becomes redundant, the Flory–Huggins expression,[34] $\ln(\Omega/\Omega^*) = -\sum_x n_x \ln \phi_x$, where ϕ_x is the volume fraction of component x, is recovered as expected.

Finally, within the mean-field approximation the interaction energy is given by

$$\beta U = \frac{1}{2} \sum_{i=1}^{M} L_i \sum_A \sum_{A'} \sum_B \sum_{B'} \phi_{Ai} P_{ABi} \chi_{BB'} \langle P_{A'B'i} \phi_{A'i} \rangle \quad (5)$$

where $\langle x_i \rangle \equiv \sum_{i'=1}^{M} \lambda_{ii'} x_{i'}$ and ϕ_{Ai} is the volume fraction of species A in layer i. In the case of nearest-neighbor interactions only, the sum over i' in the definition of $\langle x_i \rangle$ contains at most three terms. In eq 5, $\chi_{BB'}$ denotes the Flory–Huggins interaction parameter,[34] traditionally defined as $\chi_{BB'} = \beta z[\epsilon_{BB'} - (\epsilon_{BB} + \epsilon_{B'B'})/2]$, where $\epsilon_{BB'}$ is the interaction energy on a site–volume basis between species A in state B and species A′ in state B′. In expressions such as eq 5, the state summation variable B is always associated with the species summation variable A, B′ summed with A′, etc. The reference interaction energy U^* becomes nonzero in the presence of two different species in the separated-polymer reference system as given by eq A.5.2 in ref 27.

Equilibrium Distributions. The selection of the most important term in the partition function specifies one particular state and one particular conformational distribution, referred to as the equilibrium distributions. The aim is to obtain expressions of the *state* equilibrium distribution as well as of the *segment* equilibrium distribution, the latter being uniquely determined by the conformational equilibrium distribution.

The state distribution $\{P_{ABi}\}$ is given by the implicit set of nonlinear equations

$$P_{ABi} = \frac{X_{AB}}{\sum_B X_{AB}},$$

$$X_{AB} \equiv g_{AB} \exp[-\beta U_{AB} - \sum_{A'} \sum_{B'} \chi_{BB'} \langle P_{A'B'i} \phi_{A'i} \rangle] \quad (6)$$

valid for all species, states, and layers. The numerator gives the weight of species A in layer i to be found in state B, the denominator being a normalization factor. As expected, eq 6 shows that a state is favored by high degeneration, low internal energy, and a favorable interaction (small χ) with neighboring segments.

The expression for the segment distribution is more complex, due to the connectivity of the chains and to the fact that segments of a chain may reside in different layers. The determination of the segment distribution requires (i) an expression of the relative free energy of an unconnected segment being located in a layer and (ii) a method for taking into account the constraint that two connected segments in a chain have to be located in the same or in two adjacent layers. The former is given by the species potential, which may be derived from the partition function and the packing constraints. The species potential u_{Ai} can be divided into two parts, one species independent, u'_i, and the other dependent on the species, u_{Ai}^{int}, according to

$$u_{Ai} = u'_i + u_{Ai}^{int} \quad (7)$$

If the species potentials are defined with respect to the bulk solution, i.e., if $u_A^b = 0$, then the two terms are given by

$$\beta u'_i \equiv \alpha_i + \sum_x \frac{\phi_x^b}{r_x} + \frac{1}{2} \sum_{A'} \sum_{A''} \sum_{B'} \sum_{B''} \phi_{A'}^b P_{A'B'}^b \chi_{B'B''} P_{A''B''}^b \phi_{A''}^b$$

$$\beta u_{Ai}^{int} \equiv \sum_B \left[P_{ABi} \left(\beta U_{AB} + \ln \frac{P_{ABi}}{g_{AB}} \right) - P_{AB}^b \left(\beta U_{AB} + \ln \frac{P_{AB}^b}{g_{AB}} \right) \right] + \sum_{A'} \sum_B \sum_{B'} \chi_{BB'} (P_{ABi} \langle P_{A'B'i} \phi_{A'i} \rangle - P_{AB}^b P_{A'B'}^b \phi_{A'}^b) \quad (8)$$

where P_{AB}^b is the fraction of species A in bulk which is in state B, as given by a relation similar to eq 6. The species-independent potential u'_i, related to the lateral pressure in a continuous model, ensures that by a suitable choice of α_i the space is completely filled at layer i. In bulk, u' becomes zero. The species-dependent term u_{Ai}^{int} has two contributions: the internal free energy for species A in layer i being diminished by the corresponding quantity in bulk, and the mixing energy for species A in layer i being diminished by the mixing energy for species A in bulk. In both cases, averages are taken over the relevant state distributions. At distances far from the micellar center, P_{ABi} approaches P_{AB}^b, ϕ_{Ai} approaches ϕ_A^b, and hence u_{Ai}^{int} becomes zero.

The second aspect of determining the segment distribution is to take into account the chain connectivity. If only monomers are present, the volume fraction ϕ_{Ai} of monomer A in layer i is related only to the bulk volume fraction ϕ_A^b according to

$$\phi_{Ai} = G_{Ai}\phi_A^b \tag{9}$$

where the weighting factor G_{Ai} for species A in layer i is given by

$$G_{Ai} = \exp(-\beta u_{Ai}) \tag{10}$$

since the species potentials were defined to be zero in bulk. The matter becomes more complex for polymers. However, using a matrix method, the *segment* distribution as expressed in terms of n_{xsi}, the number of sites in layer i occupied by segments of rank s belonging to component x, is given by

$$n_{xsi} = C_x\{\Delta_i^T\cdot[\prod_{s'=r_x}^{s+1}(\mathbf{W}^{t(x,s')})^T]\cdot\mathbf{s}\}\{\Delta_i^T\cdot[\prod_{s'=2}^{s}\mathbf{W}^{t(x,s')}]\cdot\mathbf{p}(x,1)\} \tag{11}$$

where C_x is a normalization factor (here determined by the bulk volume fraction of component x), $\mathbf{W}^{t(x,s)}$ a tridiagonal matrix comprising elements which contain factors describing the lattice topology and weighting factors for the segment of rank s belonging to component x, and $\mathbf{p}(x,1)$ a vector describing the distribution of the first segment of component x in the layers, with Δ and $\mathbf{s}$ being elementary column vectors. From n_{xsi} the segment volume fractions are easily obtained. The *species* volume fraction ϕ_{Ai}, needed in eq 8, is given by

$$\phi_{Ai} = \frac{1}{L_i}\sum_x\sum_{s=1}^{r_x}\delta_{A,t(x,s)}n_{xsi} \tag{12}$$

where the Kronecker δ only selects segments of rank s of component x if they are of type A. Thus, given the species potentials u_{Ai}, the species volume profiles ϕ_{Ai} are obtained by eqs 10–12, these equations together with eqs 7 and 8 constituting an implicit set of nonlinear equations for the segment distributions.

Micelle Formation. The micellar solution is (hypothetically) divided into spherical subsystems (cells), each of which contains one micelle and its accompanying solution. The volume of the subsystem V_s is simply the inverse micellar number density. The excess free energy A_s of a subsystem contains two parts: A^σ, which is the free energy associated with the formation of a micelle fixed in space in contact with the bulk solution, and the mixing entropy, as given by[25]

$$\beta A_s = \beta A^\sigma + \ln(V_m/V_s) \tag{13}$$

where V_m is the volume of the micelle. A necessary requirement for stable micelles at equilibrium is that the positive A^σ be balanced by the favorable mixing entropy of the micelle, implying that $A_s = 0$. Given that the equilibrium state and the segment distributions are determined, A^σ is obtained from by

$$A^\sigma = A - A^* - \sum_x n_x(\mu_x - \mu_x^*) \tag{14}$$

where $A - A^*$ is given by eq 2. In eq 14, $\mu_x - \mu_x^*$ denotes the difference between the chemical potential of component x in bulk and in the reference state, which is given by

$$\beta(\mu_x-\mu_x^*) = r_x\sum_A\sum_B\phi_{Ax}^*\left\{P_{AB}^b\left[\beta U_{AB} + \ln\frac{P_{AB}^b}{g_{AB}}\right] - P_{AB}^*\left[\beta U_{AB} + \ln\frac{P_{AB}^*}{g_{AB}}\right]\right\} + \ln\phi_x^b + 1 - r_x\sum_{x'}\frac{\phi_{x'}^b}{r_{x'}} - \frac{r_x}{2}\sum_A\sum_{A'}\sum_B\sum_{B'}[(\phi_A^b-\phi_{Ax}^*)P_{AB}^bx_{BB'}P_{A'B'}^b(\phi_{A'}^b-\phi_{A'x}^*) + \phi_{Ax}^*\phi_{A'x}^*x_{BB'}(P_{AB}^*P_{A'B'}^*-P_{AB}^bP_{A'B'}^b)] \tag{15}$$

where ϕ_x^b denotes the volume fraction of component x and ϕ_{Ax}^* the volume fraction of species A in component x.

An important quantity is the excess number of segments of component x in the subsystem, defined as

$$\Gamma_x = \sum_{i=1}^{M}L_i[(\sum_{s=1}^{r_x}\phi_{xsi}) - \phi_x^b] \tag{16}$$

where $\phi_{xsi} = n_{xsi}/L_i$. The excess number of polymer molecules will be referred to as the aggregation number of the micelle, $N_{agg} = \Gamma_{polymer}/r_{polymer}$. Given $\Gamma_{polymer}$, the micellar volume is approximated by

$$V_m = \frac{\Gamma_{polymer}}{\phi_{polymer,i=1} - \phi_{polymer}^b} \tag{17}$$

Finally, the total volume fraction of component x in the subsystem, $\phi_{x,tot}$ (equal to the stochiometric concentration of x in the micellar solution), is the sum of the excess and bulk volume fractions according to

$$\phi_{x,tot} = \Gamma_x/V_s + \phi_x^b \tag{18}$$

Thus, on the basis of a selected bulk composition, the numerical procedure involves the computation of the equilibrium state and segment distributions according to eqs 7, 8, and 10–12 and of the excess free energy of the subsystem from eq 14. Equation 16 is then used to compute the amount of excess polymer, eq 17 to obtain the micellar volume, and eq 13 to obtain the volume of the subsystem, with the total composition being calculated finally from eq 18. Any change in the bulk composition leads to a change in the total concentration, with concomitant change in the micellar structures, or possibly to there being no micelles formed at all. The lowest total polymer concentration at which stable micelles exist (which requires $A^\sigma > 0$ and $\partial A^\sigma/\partial N_{agg} < 0$) will be referred to as the critical micelle concentration (cmc).

Phase Equilibrium in a Homogeneous System. Binodal (coexisting) curves, as well as spinodal curves of homogeneous polymer–solvent systems, have been calculated in order to relate the cmc curves to the phase stability. The location of the binodal curves was obtained with the stipulation that the chemical potential of each component given by eq 15 be the same in all the coexisting phases, whereas the location of the spinodal curve was obtained with the stipulation that the chemical potential of a component attain an extreme value.

III. Polymer Model

Polymers. The PEO–PPO–PEO triblock copolymers are known by different trademarks, Pluronic, Proxanol, and Synperonic. Pluronic polymers with differing central molecular mass of the PPO unit ($M_{PPO} \approx$ 950–4000) and with differing fraction of EO (10–90 wt %) are available. We retain M_{PPO} and the fraction of EO as the two independent parameters that describe the composition of the Pluronic polymers. Table I gives the trade abbrevi-

Table I. Trademark[a] and Composition of Each of the Pluronic Block Copolymers Studied

trademark	M_{PPO}[b]	wt % EO[b]	composition
F127	4000	70	$(EO)_{99}(PO)_{65}(EO)_{99}$[c]
P85	2250	50	$(EO)_{25}(PO)_{40}(EO)_{25}$
P95[d]	2750	50	$(EO)_{31}(PO)_{47}(EO)_{31}$
P105	3250	50	$(EO)_{37}(PO)_{56}(EO)_{37}$
P104	3250	40	$(EO)_{25}(PO)_{56}(EO)_{25}$
P103	3250	30	$(EO)_{16}(PO)_{56}(EO)_{16}$

[a] BASF Wyandotte Chemical Corp. [b] Data from the manufacturer. [c] Composition from previous investigation.[17] [d] Not commercially available.

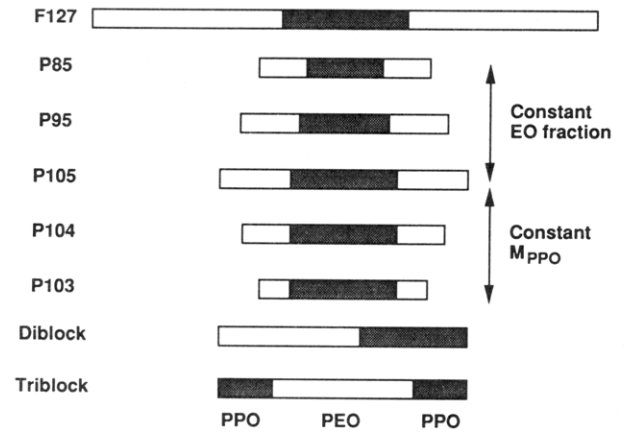

Figure 2. Schematic illustration of the molecular structure of the Pluronic triblock copolymers, as well as of di- and triblock copolymers of the same composition as Pluronic P105, studied. The PEO blocks are represented by open areas and the PPO blocks by shaded areas. The length of each area is proportional to the number of monomers of the block.

ations, and Figure 2 shows schematically the Pluronic block copolymers used in the present investigation. The Pluronic F127 block copolymer was selected due to the existence of experimental data and previous model calculations. In addition, two different series of Pluronic polymers were examined. In the series P85–P95–P105, M_{PPO} was increased when the fraction of EO was kept constant, whereas in the series P105–P104–P103, the fraction of EO was reduced when M_{PPO} was kept constant.

It was reasoned that the molecular structure affects the aggregation behavior of block copolymers. In order to examine this effect, a PEO–PPO diblock and a PPO–PEO–PPO triblock copolymer, both having the *same* overall composition as P105, were considered (Figure 2). (PPO–PEO–PPO triblock copolymers are commercially available, but only with a lower EO content than that considered here, making them nonsoluble in water.)

Interaction Parameters. The calculations for the model require a knowledge of the internal energy, U_{AB}, and the degeneration, g_{AB}, of all states of all species, as well as of the interaction parameters between all pairs of species in the different states, $\chi_{BB'}$. These parameters, given in Table II, were obtained previously in independent investigations of simpler systems through fitting calculated phase diagrams to experimental ones. Since aqueous solutions of both PEO and PPO display a lower consolute point, both the EO and PO segments are modeled with internal states, although of differing polarity. The parameters describing the internal degrees of freedom of EO, as well as the EO–water interaction, were obtained by fitting the theoretical PEO–water phase diagram[26,35] to the experimental one[36] (Figure 3a), the same procedure being used for the corresponding PO and PO–water interaction parameters[27,37] (Figure 3b). The remaining

Table II. Internal State Parameters (U_{AB} and g_{AB}) and Flory–Huggins Interaction Parameters ($\chi_{BB'}$) of the Theoretical Model (Energy in kJ mol^{-1})

species	state	state no.	U_{AB}	g_{AB}
water		1	0	1
EO	polar	2	0[a]	1[a]
	nonpolar	3	5.086[a]	8[a]
PO	polar	4	0[b]	1[b]
	nonpolar	5	11.5[b]	60[b]

	$kT\chi_{BB'}$			
state no.	2	3	4	5
1	0.6508[a]	5.568[a]	1.7[b]	8.5[b]
2		1.266[a]	1.8[c]	3.0[c]
3			0.5[c]	−2.0[c]
4				1.4[b]

[a] From the fit to the experimental data of the binary PEO–water phase diagram (see refs 26 and 35 and Figure 3a). [b] From the fit to the experimental data of the binary PPO–water phase diagram (see ref 27 and Figure 3b). [c] From the fit to the experimental data of the ternary PEO–PPO–water phase diagram (see refs 29 and Figure 4). The corresponding values of the old set are $kT\chi_{24} = kT\chi_{35} = 0.0$ kJ mol^{-1} and $kT\chi_{25} = kT\chi_{34} = 1.3$ kJ mol^{-1}.[17]

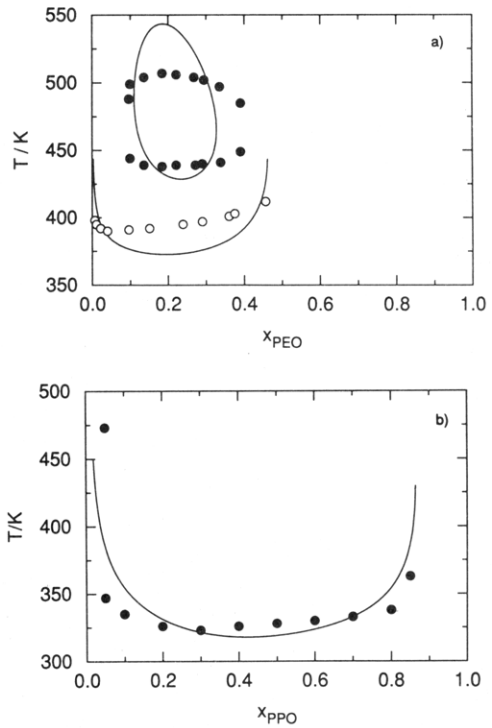

Figure 3. Phase diagram of the binary (a) PEO–water and (b) PPO–water systems. The experimental data are from (a) Saeki et al.,[36] $M_{PEO} = 2290$ (filled circles) and 8000 (open circles) and (b) Malcom et al.[37] $M_{PPO} = 440$ (filled circles). The calculated two-phase boundaries (solid curves) were obtained from eq 15 employing $r_{PEO} = 52$, 182, and $r_{PPO} = 7$, respectively, and the relevant parameters as given in Table II. The two-phase regions are either enclosed or are above the curves. The unit on the abscissa is the weight (experimental) or volume (calculated) fraction.

four EO–PO interaction parameters were obtained by fitting calculated PEO–PPO–water phase diagrams to experimental ones using the above-mentioned EO, EO–water, PO, and PO–water parameters[29] (Figure 4). A different set of EO–PO interaction parameters was used in previous model calculations of the adsorption[30,31] and micellization[17] of Pluronic polymer in aqueous solution. This set was constructed in an ad hoc fashion and resulted in a smaller effective EO–PO repulsion. As will be shown below, the new set used here reduces the tendency toward phase separation and micellization and increases

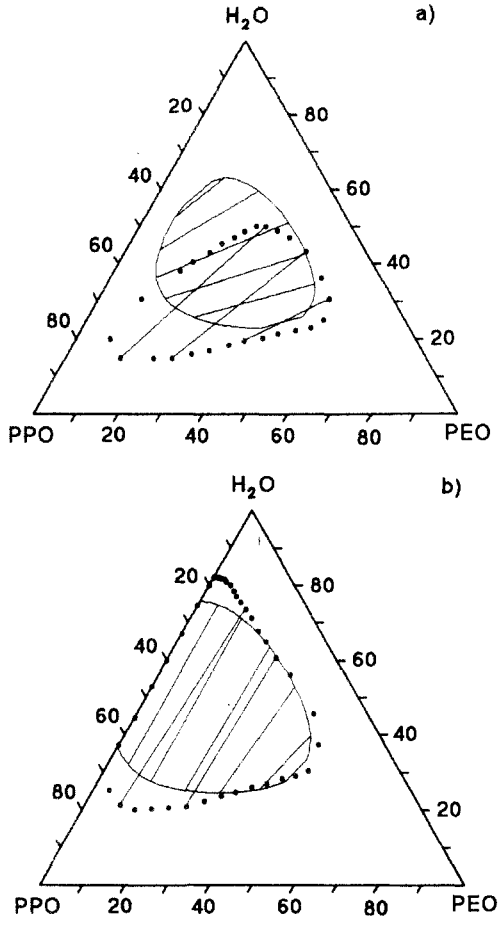

Figure 4. Phase diagram with tie lines for the ternary PEO–PPO–water system at (a) 298 K and (b) 326 K. Experimental data are from Malmsten et al.[29] for M_{PEO} = 600 and M_{PPO} = 400 (filled circles and solid tie lines). The calculated two-phase boundaries (solid curves and solid tie lines) were obtained from eq 15 employing r_{PEO} = 14 and r_{PPO} = 7, the parameters being given in Table II. The unit on the three axes is weight (experimental) or volume (calculated) percent.

the PEO–PPO segregation when structures have been formed.

An initial investigation of the usefulness of the two sets of EO–PO interaction parameters was performed by using the measured cloud-point curve for PE6200 by Tiberg et al.[30] Figure 5 shows the experimental cloud-point curve as well as two theoretically obtained coexisting curves. The latter two were obtained using the same EO, EO–water, PO, and PO–water parameters but different EO–PO interaction parameters. It is evident that, whereas the former set of EO–PO parameters reproduces the experimental phase diagram for only very small polymer volume fractions and fails drastically at higher volume fractions (dashed curve), the new set has a qualitatively correct behavior (solid curve) with an agreement similar to that of the underlying PEO–water and PPO–water phase diagrams (cf. Figure 3).

IV. Results and Discussion

Pluronic F127. At sufficiently low polymer concentration, the polymers generally occur as single entities. As the polymer concentration increases above a certain concentration, termed the critical micellar concentration, micelles are formed. In Figure 6, the volume fraction of the free polymer (referred to as the bulk volume fraction in the theoretical section) and the volume fraction of the polymer in micelles at two different temperatures for Pluronic F127 as a function of the total (stochiometric)

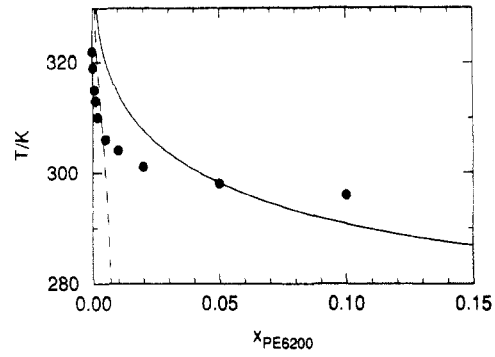

Figure 5. Phase diagram for the binary Pluronic PE6200–water system. The experimental data, representing the cloud-point curve, are from Tiberg et al.[30] (solid circles). The calculated two-phase boundary is obtained from eq 15, employing the polymer composition $(EO)_6(PO)_{37}(EO)_6$ and parameters given in Table II (solid curve). The corresponding phase boundary obtained with the old set of EO–PO interaction parameters is also given (dashed curve). The two-phase region is above the curve. The unit on the abscissa is the weight (experimental) or volume (calculated) fraction.

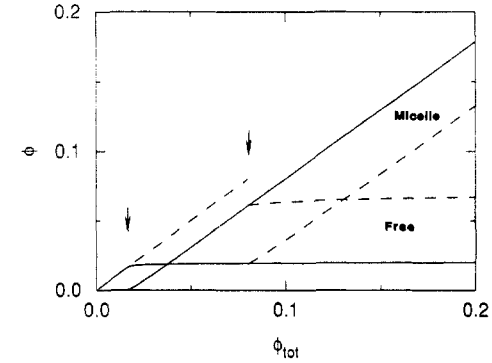

Figure 6. Calculated volume fraction of free polymers and of polymers in micelles versus the total polymer volume fraction (ϕ_{tot}) for Pluronic F127 at 330 K (solid curves) and 315 K (dashed curves). The arrows indicate the locations of the cmc's.

polymer concentration are given. The theory predicts that the cmc will have a clear location and that as the total concentration increases above the cmc the free polymer concentration rises very weakly. Thus, the chemical potential of the polymer remains nearly constant and almost all the new polymers are aggregated. The nearly constant polymer activity is analogous to what has been found for the micellization of nonionic surfactants[38] and in previous model calculations of polymer solutions.[18,25] Figure 6 shows that when the cmc is reached, the concentration of micelles becomes finite and the concentration of free polymers displays a dip. The magnitude of the dip increases with falling temperature and is only visible at lower temperatures.

Figure 6 also shows that the cmc is strongly reduced as the temperature increases. A 15 K increase causes a 4-fold reduction in the cmc. This strong temperature dependence originates from the deterioration of the solvent conditions as the temperature increases (cf. Figure 3). In Figure 7, the influence of the temperature on the calculated cmc is shown for a broad temperature range (solid curve). The figure confirms there is a strong temperature dependence over the whole range, and at the higher temperature the dependence is very pronounced. Figure 7 also shows the free polymer concentration at the cmc (dotted curve). At temperatures below ≈320 K, the concentration of the micelles at the onset of micellization begins to be considerable. The calculated coexistence curve is likewise shown in the figure (dash-dotted curve) and is located 20–30 K above the cmc curve.

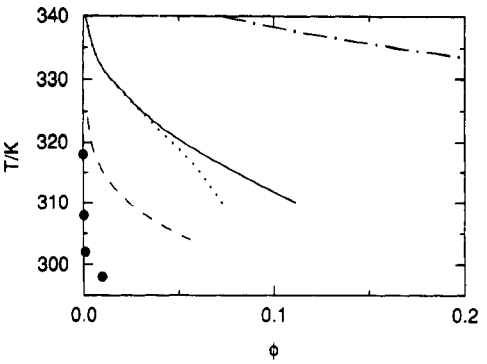

Figure 7. Critical micelle concentrations for Pluronic F127 at different temperatures. Experimental data are from Linse and Malmsten[17] (filled circles), calculation (solid curve), and calculation with the old EO–PO interaction parameters (dashed curve). Also shown are the calculated volume fraction of free polymers at cmc (dotted curve) and the calculated coexistence curve (dash-dotted curve). The unit on the abscissa is the weight (experimental) or volume (calculated) fraction.

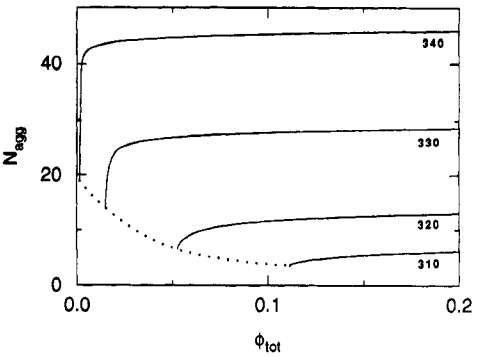

Figure 8. Calculated micellar aggregation number (N_{agg}) versus total polymer volume fraction (ϕ_{tot}) at different temperatures (solid curves) and the aggregation number at cmc (dotted curve) for Pluronic F127.

The strong temperature dependence of the cmc has been observed experimentally in a number of Pluronic systems.[7,8,11,12,17] The direct comparison with experimental cmc data for Pluronic F127[17] in Figure 7 shows the calculated cmc curve to be qualitatively correct but to appear at ≈30 K too high temperature. In this respect, the cmc curve previously obtained with the former EO–PO interaction parameters (dashed curve) seems to be more satisfactory; it is only displaced ≈15 K.

There are at least three concurrent factors involved in the 30 K discrepancy. First, and probably the most important one, is the fact that commercial Pluronic polymers are polydisperse, which is often manifested by an unclear location of the cmc. Typically, the ratio of the weight average to the number average is 1.2, and in addition there is composition dispersion. Since the experimental cmc is governed by the hydrophobic branch of the mass and composition distribution, the onset of micellization occurs at a temperature lower than that expected for a monodisperse polymer sample. Second, since lattice theory is unable to fully reproduce either the flat region of the intermediate polymer fractions or the steep rise of the low and high polymer fractions in the binary phase diagrams (see Figure 3), the fitted parameters have been selected to give the best overall fit of the coexistence curves. As a consequence, at a low polymer concentration the fitted coexistence curve is located at a higher temperature than the experimental one. The consequences are similar for the Pluronic PE6200 triblock copolymer at low polymer concentration where the calculated coexistence curve appeared at a higher temperature than the experimental cloud-point curve (Figure 5). Moreover, micellization and the phase separation of nonaggregated polymers are responses to a common cause. In the case of both, as the chemical potential rises due to increased polymer concentration, the rate of increase of the chemical potential is reduced by the formation of micelles (cf. Figure 6) or it ceases with phase separation. The third factor involved in the 30 K discrepancy concerns the fact that the PO–water interaction parameters were fitted using short PPO chains in which the hydroxyl end groups play a role. A slightly more repulsive PO–water interaction should have been used here, which would have brought the calculated and experimental curves closer to one another.

Furthermore, the calculated *coexistence* curve obtained for PE6200 at low polymer concentration using the old EO–PO parameters appears at a lower T (and agrees better with the experimental data) than the corresponding curve based on the new parameters (Figure 5). This is consistent with that the calculated cmc curve based on the old parameter set appears at a lower T (and, perhaps fortuitously, is in better agreement with experimental data) than the curve obtained using the new parameters. Thus, at the present stage of investigation the old set of EO–PO parameters appears to better reproduce the experimental cmc–temperature dependence. However, the situation might appear different in a more refined description of the system.

The aggregation number of the Pluronic micelles is another quantity of considerable interest. In Figure 8, the calculated aggregation number obtained from eq 16 is shown as a function of the total polymer concentration at various temperatures. Within the lower temperature range, in which the cmc is high, the micelles are predicted to be small at the cmc and remain fairly small as the total polymer concentration increases. At higher temperature, on the other hand, the micelles are larger at the cmc and grow rapidly as soon as the cmc is exceeded, and the aggregation number levels off soon as the total polymer concentration increases further.

Experimentally, the aggregation number can be obtained by static light scattering or fluorescence quenching measurements for example. It is clear from earlier work that an increase in temperature results in a strong increase in aggregation number, although the experimental values obtained for the aggregation number vary considerably.[2–6,8–13] For example, for Pluronic F127 close to the cmc the following has been reported: (N_{agg}, t/°C) = (3.2, 35), (9.4, 40), (12.0, 45),[10] (N_{agg}, t/°C) = (6, 10), (15, 30), (20, 35), (44, 40),[11] and (N_{agg}, t/°C) = (30, 25).[13] Disregarding the temperature shift of ≈30 K already discussed, there is a satisfactory agreement between the experimental and the calculated aggregation number, where $N_{agg} \approx 5$–10 at the lower temperature and $N_{agg} \approx 30$–45 at the higher temperature (at the latter temperature the plateau values of the calculated aggregation number are employed, since it is unlikely that the concentration of the prepared systems would fall in the narrow range in which the steep rise appears). A more detailed comparison is hampered by the spread found in the experimental data due to the uncertainty regarding the temperature dependence of the micellization and to the frequently unclear location of the cmc due to polydispersity.

The hydrodynamic radius is another quantity describing the size of the micelle. In the model calculations, the hydrodynamic radius was obtained from the polymer segment distribution using a theory proposed by Cohen Stuart et al.[39] The hydrodynamic radius is taken to be equal to the extension of a solid body which reduces the transverse flow to an extent equal to what the polymer

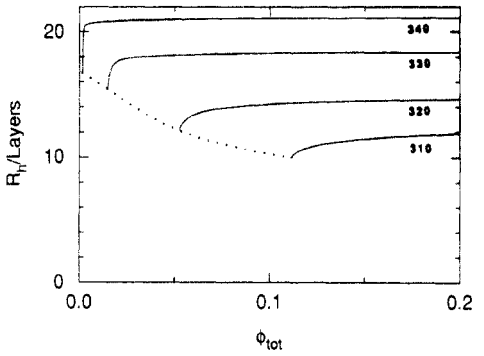

Figure 9. Calculated hydrodynamic radius (R_h) versus total polymer volume fraction (ϕ_{tot}) at different temperatures (solid curves) and the hydrodynamic radius at cmc (dotted curve) for Pluronic F127.

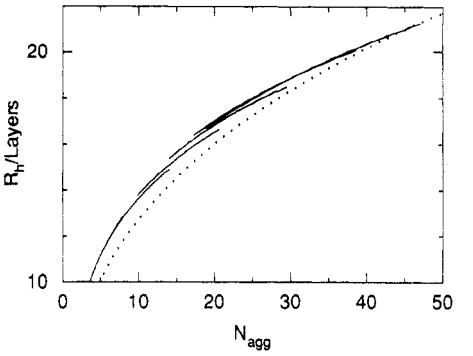

Figure 10. Calculated hydrodynamic radius (R_h) versus micellar aggregation number (N_{agg}) at different temperatures and concentrations for Pluronic F127 (solid curves). There are seven temperature curves ranging from 310 (lower left) to 340 K (upper right). The concentration varies along each temperature curve, corresponding to the cmc at the lower-left end. The dotted curve denotes the function $R_h = 5.9(N_{agg})^{1/3}$.

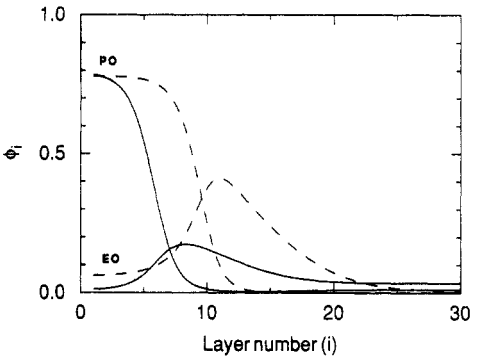

Figure 11. Calculated segment volume fraction ($\phi_{EO,i}$ and $\phi_{PO,i}$) versus layer number (i) for a total polymer volume fraction ϕ_{tot} = 0.0528 at T = 320 K (at the cmc, solid curves) and at T = 335 K (above the cmc, dashed curves) for Pluronic F127. The aggregation numbers are 6.6 and 36.2 and the hydrodynamic radii 12.2 and 19.8, respectively.

segment distribution would produce. Figure 9 indicates that the hydrodynamic radius and the aggregation number depend in a similar manner on the total polymer concentration and the temperature. At the lowest temperature, the hydrodynamic radius is equal to 10–12 layers, whereas it reaches a radius of ≈20 layers at the highest temperature considered.

Experimentally, the hydrodynamic radius can be obtained from diffusion experiments, using NMR or photon correlation spectroscopy, for example, and applying the Stokes–Einstein equation. It has been found in several studies that the hydrodynamic radius increases with micellization. The magnitude of the increase, however, varies among the studies reported.[2-6,8-10,12,40] More specifically, a hydrodynamic radius of Pluronic F127 micelles has been found to be 100 Å at 32 °C at the cmc,[10] 110 Å at 25 °C at a concentration well above the cmc,[13] and 90–95 Å for a 1% polymer concentration in the temperature range 40–50 °C.[40] In order to compare the calculated and measured hydrodynamic radii, a length has to be assigned to the lattice cell. In previous adsorption studies involving similar systems, a lattice size of ≈4 Å was shown to provide close agreement between experimental results and model predictions.[30,31] Using this value, the upper theoretical value is found to correspond to 85 Å, in reasonable agreement with the experimental findings, although somewhat too small.

An aqueous solution of Pluronic polymers has been investigated recently by use of a neutron scattering technique. From the results, it was inferred that the micellar size of Pluronic P85 increases with temperature, whereas it is basically independent of the polymer concentration.[15] This is in very close agreement with the calculated results given for Pluronic F127 in Figures 8 and 9 (and with the similar results obtained for the other Pluronic polymers investigated).

An interesting conclusion from experimental observation of EO-containing amphiphiles[41] and polymers[13] is that the EO chain contracts at elevated temperatures. In Figure 10, the calculated hydrodynamic radius is given as a function of the calculated aggregation number. The points obtained, corresponding to different temperatures and concentrations, fall close to what appears as a single universal curve. Hence, the hydrodynamic radius may be viewed as a function of the aggregation number only; it depends only indirectly through the aggregation number on temperature and concentration. Figure 10 also indicates that R_h increases more slowly than $(N_{agg})^{1/3}$ as N_{agg} increases, implying that larger micelles are more compact. For example, as N_{agg} increases from 10 to 40, the number of water molecules per EO group is reduced from 3.9 to 3.2. These numbers are obtained by considering the number of water molecules that are needed, together with the aggregated polymers, in order to fill a sphere having a radius R_h. The calculated number of water molecules per EO group compares favorably with a recent estimation of 2 to 5 water molecules per EO group perturbed by hydration at 27 °C, inferred from water self-diffusion measurements.[42] The large uncertainty range is due to difficulties in tracing the reduction in diffusion to the number of water molecules perturbed and the strength of the perturbation.

From the model, the radial volume fraction profiles for the species are obtained according to eq 12. Figure 11 shows the profiles at a total polymer fraction of 0.0528 at the cmc and at a higher temperature. In both cases, the PO segments tend to be located in the core of the micelle and the EO segments tend to primarily be located in an outer layer of the micelle. This is what one would expect from solvency, since PPO is more hydrophobic than PEO. When the temperature is increased, the size of the central PPO core likewise increases and the PEO layer is displaced to a larger radius, in accordance with the larger aggregation number and the larger hydrodynamic radius. Also, the segregation of the EO and PO segments increases with increasing temperature. This is analogous to the behavior of these polymers at hydrophobic surfaces when the amount adsorbed increases.[30]

Figure 12 shows the fraction of polar states as a function of the radial distance from the center of the micelle. The conditions are the same as in Figure 11. The fraction of polar states of both EO and PO segments increases with

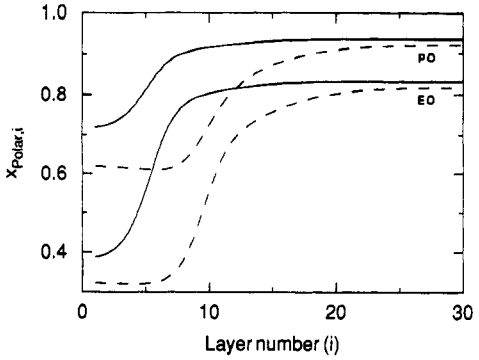

Figure 12. Calculated fraction of polar state ($x_{polar,i}$) versus layer number (i) for a total polymer volume fraction ϕ_{tot} = 0.0528 at T = 320 K (at the cmc, solid curves) and at T = 335 K (above the cmc, dashed curves) for Pluronic F127.

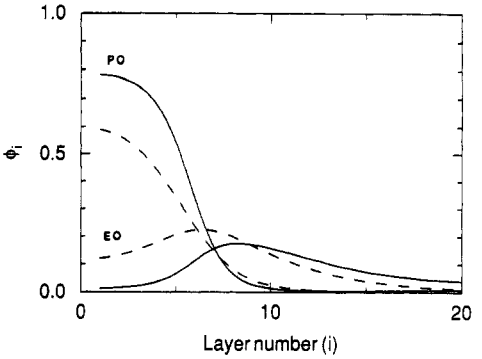

Figure 13. Calculated segment volume fraction ($\phi_{EO,i}$ and $\phi_{PO,i}$) versus layer number (i) for the cmc at a total polymer volume fraction ϕ_{tot} = 0.0528 at T = 320 K with the present EO–PO interaction parameters (solid curves) as well as at ϕ_{tot} = 0.050 and T = 304.9 K with the old EO–PO interaction parameters (dashed curves) for Pluronic F127. All other interaction parameters are the same.

the distance from the center of the micelle, as a result of conformational adaptation to an increasingly hydrophilic environment. Thus, the model predicts a micelle to consist of a hydrophobic core surrounded by a more hydrophobic shell. (Note that $x_{PO,polar} > x_{EO,polar}$ should not be interpreted as PO being more hydrophilic than EO. Although the conformations of both PEO and PPO are subdivided into one polar and one nonpolar class of conformations, their interactions with water are quite different; cf. Table II.) Figure 12 also shows that the hydrophobic core is more extended at the higher temperature, a result consistent with micelles being larger under such conditions.

The appropriateness of the models with regions of constant segment density employed in previous theoretical studies can now be evaluated. Whereas the density profile of the hydrophobic segments appears to be reasonably approximated by a uniform density in the core region, the assumption of a constant EO density in the outer layer seems less valid. In this respect, Halperin's use of the Daoud–Cotton model for star polymers, which yields a $r^{-4/3}$ density dependence of the hydrophilic block in the corona, is more realistic.[20] Also, for a larger aggregation number, resulting in a more severe stretching of the hydrophobic part of the polymers, the number of hydrophilic segments in the core is not negligible, this free energy cost thus needing to be considered.

Finally, both the aggregation number and the hydrodynamic radius of the present model calculations represent a significant improvement over those reported earlier. In terms of the old EO–PO parameters, the largest aggregation number in the temperature range 305–325 K (Figure 3 in ref 17) was 20–23, as compared with 30–45 for the corresponding temperature range (320–340 K; cf. Figure 7) in the present study. Also, in terms of the old parameters, the aggregation number at the cmc increased only from 7 to 9, as compared with an increase from 7 to 19 for the same temperature ranges in the present study. Moreover, the upper limit of the hydrodynamic radius was 70–75 Å (Figure 4 in ref 17) as compared with 80–85 Å here. Also as the aggregation number, the range of the hydrodynamic radius at cmc was smaller. In Figure 13 the volume fraction profiles obtained with the present and with the old set of EO–PO interaction parameters are shown. Both sets of profiles are calculated at the cmc and at similar total polymer concentration, viz. ϕ_{tot} = 0.0528 giving N_{agg} = 6.6 and R_h = 12.2, and ϕ_{tot} = 0.050 giving N_{agg} = 6.6 and R_h = 13.5, respectively. Clearly, the reduced free energy cost of the EO–PO contacts in the former interaction set strongly enhances the amount of EO and reduces the amount of PO in the central core (dashed curves) and consequently smooths the transition between the PO- and EO-rich regions. As a secondary effect, the amount of water in the central core increases from 20 to 30% (recall that the EO–water and PO–water interaction parameters are the same).

To summarize, the new set of EO–PO interaction parameters is the one most satisfactorily determined. Also, despite the deterioration of the cmc curve, the improvement noted in predictions of the cloud-point curve as well as of micellar size (aggregation number and hydrodynamic radius) and the more pronounced EO–PO separation in micelles with smaller water content in the core make the new set the one which yields the overall best reproduction of the experimental data.

Thus far, no direct experimental study of the structure of Pluronic micelles, for example, using neutron scattering with contrast-matching techniques, has been performed. Such experimental results would be very useful for assessing the correctness of the predicted volume fraction profiles and would provide further validation of the model calculations. Regarding the water content in the core, the prediction obtained is likely to have been too high. It has been shown previously that this type of mean-field lattice theory exaggerates the water content in hydrophobic regions.[43]

Variation of the Composition of Pluronic Triblock Copolymers. The conditions for micellization and the structure of the micelles formed were investigated for five different Pluronic block copolymers which form elements in two separate series. In the first series, P85–P95–P105, the molecular mass of the central PPO unit, M_{PPO}, is increased whereas the fraction of EO is held constant, and in the other series, P105–P104–P103, the fraction of EO is reduced, M_{PPO} being constant.

Figure 14 shows the lower section of the calculated coexistence curves of the two-phase regions of the five polymer solutions. It can be clearly seen that the coexistence curve is almost unaffected by the molecular mass, given a constant EO/PO ratio, whereas the curve shifts to a lower temperature as the EO content is reduced. The results show that the main factor determining the location of the phase separation is the relative ratio of the two differing species of the polymer, rather than the molecular mass. The molecular mass normally has an important effect on the upper part of the coexistence curve, the increase in the mixing entropy at increasing temperature contributing to the phase transition from two phases to one. The strong dependence on the EO/PO ratio is a consequence of the differing solubility of EO's and PO's at elevated temperatures (cf. Figure 3). The present

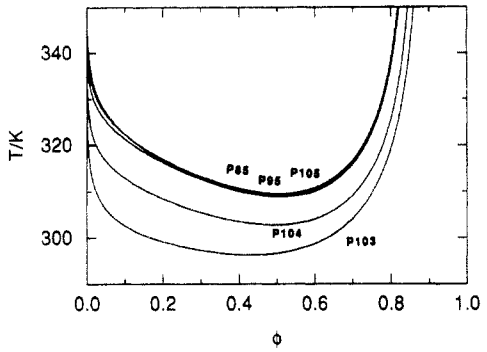

Figure 14. Calculated two-phase boundaries for Pluronic P85, P95, P105, P104, and P103. The two-phase regions are above the curves.

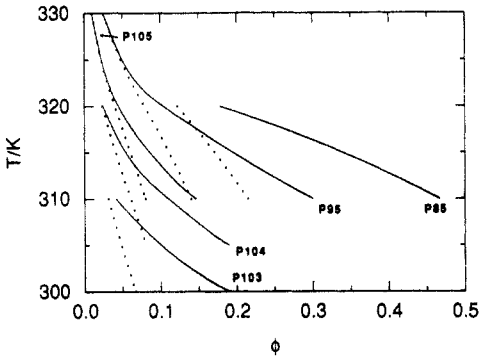

Figure 15. Calculated critical micellar concentration (solid curves) and the concentration of free polymer (dotted curves) at different temperatures for Pluronic P85, P95, P105, P104, and P103.

findings are nicely corroborated by the observed solubility of Ucon, also a EO- and PO-containing polymer, in which the tendency toward micellization is suppressed due to random EO and PO distribution along the chain. For example, an increase in the molecular mass from 3200 to 4000 for a Ucon polymer containing 50% EO (a 1% polymer solution) causes only a 1 K reduction in the cloud point. A similar temperature reduction is achieved when the EO content is lowered from 50 to only 49.5% (as inferred from ref 44).

The location of the cmc curves and the influence of the temperature differ for the two series. Figure 15 shows the cmc and the concentration of the free polymer volume fraction as a function of temperature. The calculations have been performed for an interval of 5 K, the upper temperature of each curve being the highest temperature at which stable micelles were found. Although cmc curves continue on to lower temperatures than those given, the total polymer concentration becomes higher (the model neglects micelle–micelle interactions) and the micelles become smaller as this occurs, making this region less interesting.

The most important results obtained concern the trends for the location of the cmc curves. In the series with decreasing EO fractions, P105–P104–P103, the micellization starts under conditions of decreasing temperature (the total polymer concentration being constant). This is in analogy with the phase behavior obtained. However, in the series of decreasing molecular mass and with a constant EO/PO ratio, the temperature for micellization increases (with constant polymer concentration), or alternatively, at constant temperature, the total polymer concentration at the onset of micellization increases. Thus, not only the EO/PO ratio, as with the coexisting curves, but also the polymer length influences micellization. A shorter chain makes micellization more costly.

Table III. Total ϕ_{tot} and Free ϕ_{free} Polymer Volume Fractions and the Aggregation Number N_{agg} at the Highest Temperature at Which Micelles Were Formed, T_h, as Well as the Temperature of the Coexistence Curve, T_c, Corresponding to the Free Polymer Volume Fraction at T_h

	cmc				coexistence	
polymer	T_h	ϕ_{tot}	ϕ_{free}	N_{agg}	curve: T_c	T_c-T_h[a]
P85	320	0.178	0.122	10.5	320.9	0.9
P95	330	0.0248	0.0248	23.0	330.3	0.3
P105	330	0.0101	0.0101	27.1	332.1	2.1
P104	320	0.0245	0.0236	20.6	320.2	0.2
P103	310	0.0417	0.0314	17.2	308.8	−1.2

[a] A negative T_c-T_h implies that the state point is located in the two-phase region.

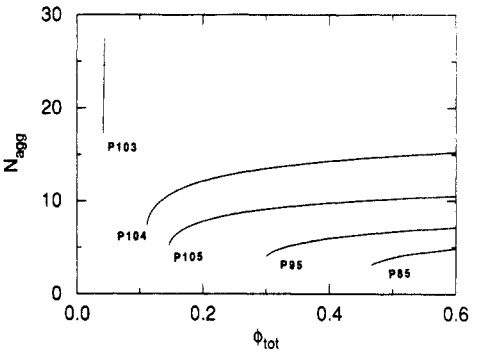

Figure 16. Calculated micellar aggregation number (N_{agg}) versus total polymer volume fraction (ϕ_{tot}) at T = 310 K for Pluronic P85, P95, P105, P104, and P103.

A second and likewise important result, shown in Figure 15, concerns the temperature range over which micelles can exist. With inclusion of the results for Pluronic F127 shown in Figure 7, the model calculations indicate that, as the polymer chain becomes shorter *or* as the EO fraction decreases, the temperature range over which micelles can be formed is reduced due to a stronger temperature dependence (smaller slope) and an increase in polymer concentration at the highest temperature at which micelles occur.

The third observation concerns the relation between the volume fraction of the free polymer at the cmc, as given in Figure 15, and the coexistence curves shown in Figure 14. For the longest and most EO-rich polymer, F127, the cmc curve is located ≈30 K below the coexistence curve (see Figure 7). However, as the polymer chain becomes shorter *or* as the EO fraction decreases, the temperature gap between the composition at coexistence and the free polymer concentration is reduced. In Table III, the total and free polymer fractions at the highest temperature at which micelles were found for each of the polymer solutions, T_h, and the temperature found at the coexistence curve for the corresponding free polymer volume fraction, T_c, are compiled. For Pluronic P105, the temperature gap $T_c - T_h$ is reduced to 2 K, whereas for P103 the highest micellization temperature lies in the metastable two-phase region. The same would probably have occurred for Pluronic P85 if a finer T grid had been used in the cmc calculations.

The variations in the aggregation number and in the hydrodynamic radius as a function of concentration and temperature for Pluronic P85, P95, P105, P104, and P103 (not shown) are similar to that obtained for F127. Table III gives N_{agg} at the cmc for the five Pluronic polymers at T_h, and Figure 16 shows N_{agg} as a function of the total polymer concentration at T = 310 K, a temperature at which all five polymers form micelles. In the two cases given by Table III and in Figure 16, as well as the case

shown in Figure 8, there is an inverse relation between the cmc and the aggregation number at the cmc, although the conditions for the three cases differ. In Figure 8 the effects of a variation in temperature at constant polymer composition, in Figure 16 the effects of varying the polymer composition at constant temperature, and in Table III the effects of varying the polymer composition at the highest micellization temperature are considered.

The almost universal behavior of the hydration radius as a function of the aggregation number is also found for P105, P104, and P103 and to a less extent for P85 and P95. The prefactor 5.9 found for Pluronic F127 (cf. Figure 10) reduces to 4.0, 3.8, and 3.5 for P105, P104, and P103, respectively. Thus, a shortening of the length of the EO blocks reduces the hydrodynamic radius for a given aggregation number and makes the micelle more compact.

Hence, the strong temperature variation of the cmc as well as of the size of the micelles formed by Pluronic F127 is also found for the other Pluronic polymers considered. The EO/PO ratio and molecular mass have a strong impact on the temperature and the cmc ranges of interest. A reduction in EO content or in molecular mass makes micelle formation less pronounced. In particular, model calculations of such small hydrophobic Pluronic polymers as L64 (M_{PPO} = 1750 and 40% EO) indicate no stable micelles. However, an aqueous solution of L64 is known to aggregate,[4,8] although it has not established whether the aggregate should be viewed as a classical micelle or as a less well-defined aggregate with extensive size and shape fluctuations.

Although the experimental difficulties in determining the micelles formed by the smaller and more hydrophobic polymers are taken into account, it is likely that the failures in the modeling of the micellization of these polymers are due to deficiencies in the model. A tentative reason for assuming this is that the cooperative effect involved in the micellization is not treated accurately enough by the mean-field approximation. As the micelles become smaller, their fluctuations in shape and size become more accentuated and a mean-field description becomes less appropriate. It should be noted, however, that the mean-field lattice model is able to predict micelle formation of short-chain surfactants.[45] In these systems, the difference in solubility of the two amphiphilic parts is much larger, resulting in tendencies being stronger for micellization and hence in the fluctuations becoming less pronounced.

In the work by Nagarajan and Ganesh, scaling relations between micellar size and polymer composition were determined for Pluronic polymers in aqueous solution.[22] They obtained, in our notation, $N_{agg} \propto (r_{PO})^{1.10}(r_{EO})^{-0.24}$, $R_{core} \propto (r_{PO})^{0.70}(r_{EO})^{-0.08}$, and $D \propto (r_{PO})^{0.07}(r_{EO})^{0.68}$, where R_{core} is the radius of the hydrophobic core and D the thickness of the hydrophilic core. The small composition range considered in the present study makes it hazardous to predict scaling relations. Nevertheless, the trends obtained are in accordance with the relations just referred to. In the present study, however, the size of the micelles as well as the cmc differed markedly from those that Nagarajan and Ganesh reported. They obtained very large aggregation numbers, typically 500–1000, as well as remarkably low critical micellar concentrations, $\phi_{cmc} < 10^{-20}$.

Variation of the Structure of Block Copolymers. Besides the effects of the polymer composition on micellization, the effects of the structural arrangement of the blocks were investigated. As shown in Figure 2, a PEO–PPO diblock copolymer and a PPO–PEO–PPO triblock copolymer of the same composition as P105 were considered. There is a difference between the two triblock copolymers in the way the segments are connected, in one of them the PPO unit being in the very center and in the other the PEO unit forming the central section.

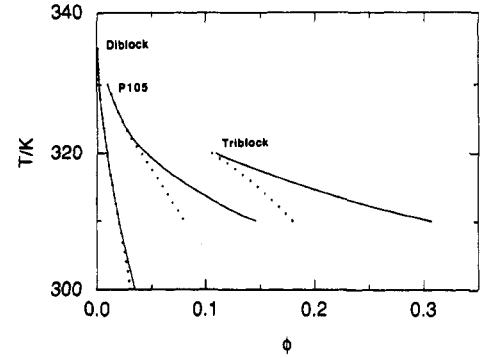

Figure 17. Calculated critical micellar concentration (solid curves) and the concentration of free polymer (dotted curves) at different temperatures for a PEO–PPO diblock, Pluronic P105, and a PPO–PEO–PPO triblock copolymer. The di- and triblock copolymers have the same composition as the Pluronic triblock copolymer; see Figure 2.

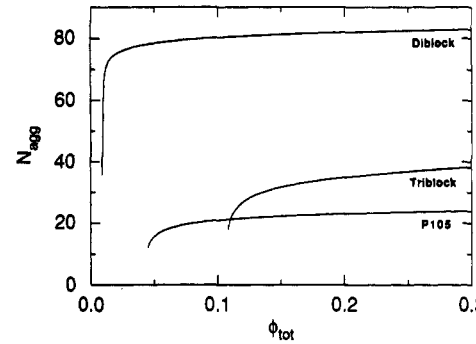

Figure 18. Calculated micellar aggregation number (N_{agg}) versus total polymer volume fraction (ϕ_{tot}) at T = 320 K for the diblock, Pluronic P105, and the triblock copolymers.

Figure 17 shows that the cmc characteristics of the three polymers vary considerably. The diblock copolymer forms micelles easiest of them all and, likewise for Pluronic F127, the cmc curve extends over a large temperature range and continues to higher temperature than given in the figure. In contrast, the triblock copolymer only forms micelles at high total polymer concentration and only within a narrow temperature range. Thus, although the three polymers possess the same solubility in the Flory–Huggins model, the tendency toward self-assembling differs drastically. In the sequence diblock–P105–triblock, the largest step is to be found between the diblock and P105, there being a 5-fold increase in the cmc, whereas the ratio of the cmc between P105 and the triblock copolymer is a factor of 2. Roughly viewed, the free energy cost of having a loop in the micellar core, a doubling of the chain flux across the PO–EO interface region, and the reduction in the length of EO tails is $\approx RT \ln 5 \approx 1.6RT$, and the additional cost of breaking the loop of the PO unit and joining together the two EO tails amounts to $\approx RT \ln 2 \approx 0.7RT$.

The consequences for the aggregation number of the molecular architecture are also profound. Figure 18 shows the aggregation number as a function of the total polymer volume fraction at T = 320 K, a temperature at which all three polymers form micelles. After the initial rise at cmc, the diblock copolymer forms micelles with $N_{agg} \approx 80$, which rises to $N_{agg} \approx 200$ at T = 335. The aggregation number of the triblock polymer resembles more that of P105. It is to be noted, however, that the micelles formed by the triblock polymer are larger, although the cmc is largest in

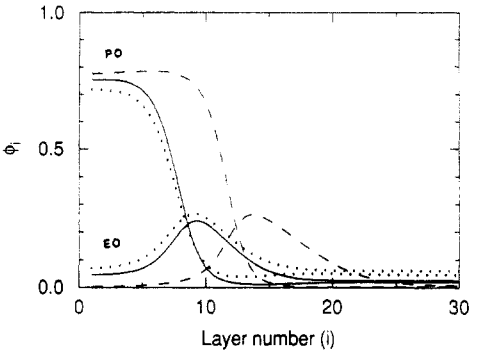

Figure 19. Calculated segment volume fraction ($\phi_{EO,i}$ and $\phi_{PO,i}$) versus layer number (i) for a total polymer volume fraction ϕ_{tot} = 0.11 at T = 320 K for the diblock copolymer (dashed curves), P105 (solid curves), and the triblock copolymer (dotted curves). The aggregation numbers are 80.5, 21.3, and 21.3, and the hydrodynamic radii 19.9, 11.5, and 14.0, respectively.

Table IV. Volume Fraction of the PEO–PPO Junction $\phi^{junction}$ in Different Layers for the Diblock, P105, and Triblock Copolymers at ϕ_{tot} = 0.11 and T = 320 K[a]

	$10^3\phi^{junction}$		
layer	diblock	P105	triblock
1	0.19	2.4	3.5
i_{max}[b]	7.8	7.1	6.6
M[c]	0.08	0.35	0.82

[a] Since there are two junctions for P105 and the triblock copolymer, the value of $\phi^{junction}$ is divided by two in these cases. [b] The layer at which $\phi^{junction}$ attains its maximum is i_{max} = 13, 7, and 7 for the diblock, P105, and triblock copolymers, respectively. [c] The outermost layer considered. The values given are equal to the free polymer volume fraction divided by $r_{polymer}$.

the case of the triblock. This breaks the relation low cmc–large N_{agg} found for the diblock copolymer–P105 pair, as well as for the Pluronic polymers of differing composition (Figure 16).

The segment volume distribution functions at T = 320 K and ϕ_{tot} = 0.11 are shown in Figure 19. Under these conditions P105 and the triblock copolymers form micelles of the same aggregation number. Here too, the diblock copolymer differs drastically from the other two copolymers. In particular, the separation of EO and PO into different domains is almost complete. Nevertheless, there are considerable differences between P105 and the triblock copolymer of the volume fraction of PO in the core. Thus, the more demanding packing constraint for the triblock polymer results in a smaller PO content in the core, whereas the simpler structure of the diblock leads to well-separated EO and PO regions.

The present lattice model also provides information about the radial location of each segment in the chain (cf. eq 11). An interesting aspect of this is the question of how well localized in space the PEO–PPO junctions are. The previous scaling approaches employed in the modeling of block copolymers assume the block junctions to be localized in a narrow interfacial region. The volume fraction profiles of the PEO–PPO junctions were determined for the diblock copolymer, P105, and the triblock copolymer at ϕ_{tot} = 0.11 and T = 320 K. The profiles tend to display a maximum at the border of the EO- and PO-rich regions. Certain aspects of these distributions are presented in Table IV. It is only in the case of the diblock copolymer that the junction is fairly well localized. The maximum volume fraction occurs in layer 12 (cf. the EO and PO volume fraction profiles in Figure 19), and the width at half-height is 5 layers. For P105, and in particular for the triblock copolymer, the junction distribution is broad and the junction density at the center of the micelle reduces to only about half of the maximum value attained in layer 7. Thus, for the triblock copolymers the assumption of a localized PEO–PPO junction seems to be less realistic.

V. Conclusions

The micellization of different block copolymers consisting of EO and PO segments was investigated on the basis of a lattice theory for polymer solutions in heterogeneous systems. The inverse temperature behavior occurring in the phase diagram of aqueous PEO and PPO solutions was taken into account by allowing the polymer segments to adopt different states depending upon the temperature and concentration of the solutions. Effective segment–segment interaction becomes both concentration and temperature dependent. All the interaction parameters employed were derived independently in previous investigations of the phase diagrams of simpler systems. In particular, a new set of EO–PO interaction parameters, obtained from ternary phase diagrams, has been employed. Thus, no adjustable parameters were involved in this study.

The results show that the theory is able to predict properties related to the micellization of Pluronic F127 in aqueous solution. The most prominent aspect found was the strong temperature dependence of the critical micellar concentration, which is closely related to the inverse temperature behavior of PEO and PPO in aqueous solution. Since an increase in temperature worsens the solvency conditions, it can be expected to reduce the cmc. Concomitant with the reduction in cmc, there is an increase in the aggregation number. In addition, at constant temperature the cmc decreases with increasing polymer length, with decreasing EO content, and with a change in the polymer structure to that of a simpler diblock copolymer.

The greatest weakness of the present model is its inability to predict the micelle formation of shorter Pluronic polymers which are known experimentally to aggregate. This deficiency can probably be traced to certain assumptions of the lattice model. A likely candidate is the mean-field approximation, which suppresses the appearance of irregular and small micelles. Another disagreement between the experimental and theoretical results is the temperature difference in the location of the cmc curves. Possible reasons for this discrepancy are the polydispersity of the experimental samples, the inability of the model to describe completely the phase behavior of the simpler binary polymer–solvent systems, and the end effects of the fitted interaction parameters.

Despite these shortcomings, the present model provides rich insight into the micellization of block copolymers. Comparison with previous theories based partly on scaling assumptions indicates rather close agreement. Moreover, possibilities for assessing certain assumptions of the respective models are thus provided. For example, the assumption of a uniform distribution of the hydrophobic block in the core seems reasonable, whereas the corresponding uniform distribution of the hydrophilic segments in the outer layer appears more questionable.

Acknowledgment. Martin Malmsten is gratefully acknowledged for his valuable comments on the manuscript. This work was supported by the Swedish Research Council for Engineering Science (TFR).

References and Notes

(1) Schmolka, I. R. J. *Biomed. Mater. Res.* **1972**, *6*, 571.

(2) Tontisakis, A.; Hilfiker, R.; Chu, B. *J. Colloid Interface Sci.* **1990**, *135*, 427.
(3) Almgren, M.; Alsins, J. *Langmuir* **1991**, *7*, 446.
(4) Bahadur, P.; Almgren, M.; Jansson, M.; Li, P.; Brown, W.; Bahadur, A. *J. Colloid Interface Sci.* **1992**, *151*, 157.
(5) Bahadur, P.; Li, P.; Almgren, M.; Brown, W. *Langmuir* **1992**, *8*, 1903.
(6) Bahadur, P.; Pandya, K.; Almgren, M.; Li, P.; Stilbs, P. *Colloid Polym. Sci.*, submitted for publication.
(7) Reddy, N. K.; Fordham, P. J.; Attwood, D.; Booth, C. *J. Chem. Soc., Faraday Trans.* **1990**, *86*, 1569.
(8) Zhou, Z.; Chu, B. *J. Colloid Interface Sci.* **1988**, *126*, 171; *Macromolecules* **1988**, *21*, 2548.
(9) Al-Saden, A. A.; Whateley, T. L.; Florence, A. T. *J. Colloid Interface Sci.* **1982**, *90*, 303.
(10) Attwood, D.; Collett, J. H.; Tait, C. J. *Int. J. Pharm.* **1985**, *26*, 25.
(11) Rassing, J.; Attwood, D. *Int. J. Pharm.* **1983**, *13*, 47.
(12) Brown, W.; Schillén, K.; Almgren, M.; Hvidt, S.; Bahadur, P. *J. Phys. Chem.* **1991**, *95*, 1850.
(13) Wanka, G.; Hoffmann, H.; Ulbricht, W. *Colloid Polym. Sci.* **1990**, *268*, 101.
(14) Brown, W.; Schillén, K.; Hvidt, S. *J. Phys. Chem.* **1992**, *96*, 6038.
(15) Mortensen, K.; Pedersen, J. S. *Macromolecules* **1993**, *26*, 805.
(16) Hurter, P. N.; Hatton, T. A. *Langmuir* **1992**, *8*, 1291.
(17) Linse, P.; Malmsten, M. *Macromolecules* **1992**, *25*, 5434.
(18) Leibler, L.; Orland, H.; Wheeler, J. C. *J. Chem. Phys.* **1983**, *79*, 3550.
(19) Noolandi, J.; Hong, K. M. *Macromolecules* **1983**, *16*, 1443.
(20) Halperin, A. *Macromolecules* **1987**, *20*, 2943.
(21) Munch, M. R.; Gast, A. P. *Macromolecules* **1988**, *21*, 1360.
(22) Nagarajan, R.; Ganesh, K. *J. Chem. Phys.* **1989**, *90*, 5843.
(23) Scheutjens, J. M. H. M.; Fleer, G. J. *J. Phys. Chem.* **1979**, *83*, 1619; **1980**, *84*, 178.
(24) Leermakers, F. A. M.; Van der Schoot, P. P. A. M.; Schutjens, J. M. H. M.; Lyklema, J. In *Surfactants in Solution*; Mittal, K. L., Ed.; Plenum Publishing Corp.: New York, 1989; Vol. 7.
(25) van Lent, B.; Scheutjens, J. M. H. M. *Macromolecules* **1989**, *22*, 1931.
(26) Karlström, G. *J. Phys. Chem.* **1985**, *89*, 4962.
(27) Linse, P.; Björling, M. *Macromolecules* **1991**, *24*, 6700.
(28) Sjöberg, A.; Karlström, G. *Macromolecules* **1989**, *22*, 1325.
(29) Malmsten, M.; Linse, P.; Zhang, K.-W. *Macromolecules* **1993**, *26*, 2905.
(30) Tiberg, F.; Malmsten, M.; Linse, P.; Lindman, B. *Langmuir* **1991**, *7*, 2723.
(31) Malmsten, M.; Linse, P.; Cosgrove, T. *Macromolecules* **1992**, *25*, 2474.
(32) Carlsson, M.; Linse, P.; Tjerneld, F. *Macromolecules* **1993**, *26*, 1546.
(33) Björling, M.; Karlström, G.; Linse, P. *J. Phys. Chem.* **1991**, *95*, 6706.
(34) Flory, P. J. *Principles of Polymer Chemistry*; Cornell University Press: Ithaca, NY, 1953.
(35) Björling, M.; Linse, P.; Karlström, G. *J. Phys. Chem.* **1990**, *94*, 471.
(36) Saeki, S.; Kuwahara, N.; Nakata, M.; Kaneko, M. *Polymer* **1976**, *17*, 685.
(37) Malcolm, G. N.; Rowlingson, J. S. *Trans. Faraday Soc.* **1957**, *53*, 921.
(38) Wennerström, H.; Lindman, B. *Phys. Rep.* **1979**, *52*, 1.
(39) Cohen Stuart, M. A.; Waajen, F. H. W. H.; Cosgrove, T.; Vincent, B.; Crowley, T. L. *Macromolecules* **1984**, *17*, 1825.
(40) Malmsten, M.; Lindman, B. *Macromolecules* **1992**, *25*, 5440.
(41) Nilsson, P. G.; Lindman, B. *J. Phys. Chem.* **1983**, *87*, 4756.
(42) Malmsten, M.; Lindman, B. *Macromolecules* **1992**, *25*, 5446.
(43) Leermakers, F. A. M.; Scheutjens, J. M. H. M. *J. Chem. Phys.* **1988**, *89*, 3264.
(44) Union Carbide, Ethylene Oxide Derivates Division, *Ucon fluids and lubricants*, 1981.
(45) Böhmer, M. R.; Koopal, L. K.; Lyklema, J. *J. Phys. Chem.* **1991**, *95*, 9569.